

# Tensor Decomposition-Based Channel Estimation and Sensing for Millimeter Wave MIMO-OFDM V2I Systems



WANG Jilin<sup>1</sup>, ZENG Xianlong<sup>1</sup>, YANG Yonghui<sup>2,3</sup>,  
PENG Lin<sup>2,3</sup>, LI Lingxiang<sup>1</sup>

(1. National Key Laboratory of Wireless Communications, University of Electronic Science and Technology of China, Chengdu 611731, China;

2. ZTE Corporation, Shenzhen 518057, China;

3. State Key Laboratory of Mobile Network and Mobile Multimedia Technology, Shenzhen 518055, China)

DOI: 10.12142/ZTECOM.202403008

<https://kns.cnki.net/kcms/detail/34.1294.TN.20240723.1657.002.html>,  
published online July 24, 2024

Manuscript received: 2024-03-01

**Abstract:** An integrated sensing and communication (ISAC) scheme for a millimeter wave (mmWave) multiple-input multiple-output orthogonal frequency division multiplexing (MIMO-OFDM) Vehicle-to-Infrastructure (V2I) system is presented, in which both the access point (AP) and the vehicle are equipped with large antenna arrays and employ hybrid analog and digital beamforming structures to compensate the path loss, meanwhile compromise between hardware complexity and system performance. Based on the sparse scattering nature of the mmWave channel, the received signal at the AP is organized to a four-order tensor by the introduced novel frame structure. A CANDECOMP/PARAFAC (CP) decomposition-based method is proposed for time-varying channel parameter extraction, including angles of departure/arrival (AoDs/AoAs), Doppler shift, time delay and path gain. Then leveraging the estimates of channel parameters, a nonlinear weighted least-square problem is proposed to recover the location accurately, heading and velocity of vehicles. Simulation results show that the proposed methods are effective and efficient in time-varying channel estimation and vehicle sensing in mmWave MIMO-OFDM V2I systems.

**Keywords:** MIMO-OFDM Vehicle-to-Infrastructure (V2I) systems; ISAC; time-varying channel estimation; CANDECOMP/PARAFAC (CP) decomposition

**Citation** (Format 1): WANG J L, ZENG X L, YANG Y H, et al. Tensor decomposition-based channel estimation and sensing for millimeter wave MIMO-OFDM V2I systems [J]. *ZTE Communications*, 2024, 22(3): 56 – 68. DOI: 10.12142/ZTECOM.202403008

**Citation** (Format 2): J. L. Wang, X. L. Zeng, Y. H. Yang, et al., “Tensor decomposition-based channel estimation and sensing for millimeter wave MIMO-OFDM V2I systems,” *ZTE Communications*, vol. 22, no. 3, pp. 56 – 68, Sept. 2024. doi: 10.12142/ZTECOM.202403008.

## 1 Introduction

Due to the large available bandwidth and small wavelength, millimeter wave (mmWave) communication technology has received much attention. To compensate for the severe path loss of mmWave systems, large antenna arrays are usually used at the transmitter and receiver to provide sufficient beamforming gain for mmWave communications. However, to obtain the directional beam gain, accurate channel information needs to be realized by channel estimation<sup>[1-5]</sup>.

In recent years, the millimeter-wave channel estimation problem has been widely investigated. By exploring its sparsity in the angular domain, the millimeter-wave channel estimation problem is equivalent to a sparse signal recovery problem, which can be solved with the help of compressive sensing tools<sup>[6]</sup>. It has been shown in Refs. [6 – 7] that a sub-

stantial reduction in training overhead can be achieved via compressed sensing methods. Also, a low-complexity channel estimation algorithm was proposed by exploiting the strongest angles of arrival in mmWave channels<sup>[8]</sup>. Besides, the authors in Ref. [9] exploited the delay-domain sparsity of wideband channels and a sparse signal recovery-based scheme was proposed for channel estimation. Moreover, tensor-based channel estimation was introduced in Refs. [10] and [11], which exploited the multi-dimensional characteristics of the mmWave multiple-input multiple-output (MIMO) channels with the low-rank property. Specifically, the received signal was organized to a third-order tensor, and a CANDECOMP/PARAFAC (CP) decomposition-based method was proposed to estimate channel parameters including angles of departure/arrival (AoDs/AoAs), time delays, and fading coefficients. However, in practice, the wireless

transceivers may have high-speed relative movements, e.g., high-speed trains<sup>[12]</sup>, unmanned aerial vehicles (UAVs)<sup>[13]</sup> and vehicle-to-everything (V2X) networks<sup>[14]</sup>. In particular, the high-speed relative movements introduce severe Doppler effects on the multiple propagating paths and result in a time-varying multipath mmWave channel. To enable high data rate transmissions for high mobility, the time-varying mmWave channel estimation has been studied in Refs. [15 – 16]. In Ref. [15], the time-varying channel estimation was divided into two separate stages including AoA/AoD estimation and followed by a path gain estimation. Also, by rearranging the received signal, a canonical polyadic decomposition (CPD)-based method was developed in Ref. [16] to estimate the time-varying mmWave channel.

The relative position and relative velocity of the transmitter and the receiver are known as channel estimations that give information on the AoA/AoD and the Doppler shift. Furthermore, the location information may be utilized as a stand-in for channel information to enable beamforming. This means that if the position of the mobile station (MS) is known, the AP can steer its transmission to the MS, either directly or via a reflective path. Further, the velocity information can be utilized to predict the position of MS, which helps the AP to perform beam alignment efficiently. This leads to synergies between communication and sensing. Previous works in Refs. [17 – 19] for millimeter waves and in Refs. [20 – 21] for massive MIMO explored using 5G techniques to acquire location and orientation. Ref. [17] considered estimating and tracking AoA by beam switching. The MS localization was formulated as a hypothesis-testing problem in Ref. [18]. Besides, Ref. [19] obtained meter-level positioning accuracy by measuring received signal strength levels. In the massive case, Ref. [20] addressed the estimation of angles, while Ref. [21] considered the joint delay and AoD/AoA estimation in the line-of-sight (LoS) conditions, and the impact of errors in delay and phase shifters was also analyzed.

In this paper, we consider the integrated sensing and communications for a millimeter wave MIMO-orthogonal frequency division multiplexing (MIMO-OFDM) Vehicle-to-Infrastructure (V2I) system. Specifically, we formulate the time-varying mmWave channel model for a MIMO-OFDM system and propose a novel frame structure. The received signal in the training stage is organized to a four-order tensor, and then a CP decomposition-based method is introduced to estimate the channel parameters. After the channel parameters in each AP are available, a nonlinear weighted least-square problem is proposed to recover the location, heading and velocity of the vehicle accurately.

## 2 System Model

We consider an uplink V2I mmWave OFDM system, where each access point (AP) is equipped with a uniform lin-

ear array (ULA) of  $N_r$  antennas and the vehicle is equipped with a ULA with  $N_t$  antennas. The system is assumed to operate at a carrier frequency  $f_c$  and the total number of OFDM tones (subcarriers) is  $\bar{Q}$ . The  $q$ -th subcarrier shift is  $f_q = \frac{qf_s}{\bar{Q}}$ ,

where  $f_s$  is the sampling rate. The duration time of an OFDM symbol is set to  $T_{\text{sym}}$ . The vehicle is moving at a certain speed, and the relative motion between the AP and the vehicle gives rise to the Doppler effect, which in turn leads to time-varying channels.

### 2.1 Time-Varying Channel Model

Due to the sparse scattering characteristic of mmWave channels, we adopt a geometric wideband mmWave channel model to characterize the channel between the AP and the vehicle<sup>[22]</sup>. Specifically, considering the Doppler shift caused by the vehicle's mobility, the frequency-domain mmWave channel associated with the  $q$ -th subcarrier at the  $t$ -th time instant can be expressed as follows<sup>[15, 23]</sup>.

$$\mathbf{H}_q(t) = \sum_{l=1}^L \beta_{l,l} \mathbf{a}_R(\phi_l) \mathbf{a}_T^H(\theta_l) e^{-j2\pi f_q \tau_l} e^{j2\pi \nu_l t}, \quad (1)$$

where  $L$  represents the number of signal paths,  $\beta_{l,l}$ ,  $\theta_l$ ,  $\phi_l$ ,  $\tau_l$  and  $\nu_l$  denote the complex path gain, AoD/AoA, time delay, and Doppler shift of the  $l$ -th path, respectively. The Doppler shift can be calculated as  $\nu_l = v_l f_c / c$ , where  $v_l$  is the radial velocity (i.e. the component of velocity along the line of sight to the observer) of the  $l$ -th path, and  $c$  represents the speed of light. Here we assume the path gain  $\beta_{l,l}$  remains unaltered during one OFDM frame, where the frame structure will be elaborated later. Also, we assume that the angle parameters such as AoAs and AoDs remain unchanged within the frame, as these parameters depend only on the relative positions of the AP, the vehicle, and the scatterers<sup>[2]</sup>. The steering vectors of the vehicle and the AP are represented by  $\mathbf{a}_T(\theta) \in \mathbb{C}^{N_t}$  and  $\mathbf{a}_R(\phi) \in \mathbb{C}^{N_r}$ , which are given as

$$\mathbf{a}_T(\theta) \triangleq \frac{1}{\sqrt{N_t}} \left[ 1, e^{j\frac{2\pi}{\lambda_c} d \sin(\theta)}, \dots, e^{j\frac{2\pi}{\lambda_c} d(N_t-1) \sin(\theta)} \right]^T, \quad (2)$$

$$\mathbf{a}_R(\phi) \triangleq \frac{1}{\sqrt{N_r}} \left[ 1, e^{j\frac{2\pi}{\lambda_c} d \sin(\phi)}, \dots, e^{j\frac{2\pi}{\lambda_c} d(N_r-1) \sin(\phi)} \right]^T, \quad (3)$$

where  $d$  denotes the distance between two adjacent antenna elements, and typically  $d$  is set to be half of the signal wavelength.

### 2.2 Uplink Transmission and Signal Model

We assume that hybrid analog and digital beamforming structures are employed by both the vehicle and the AP. Specifically, the vehicle and the AP are respectively equipped

with  $M_l \leq N_l$  and  $M_r \leq N_r$  radio frequency (RF) chains. At each time instant, the pilot symbol of each subcarrier  $s_q(t)$  is first precoded by a baseband precoding vector  $\mathbf{f}_{D,q}(t) \in \mathbb{C}^{M_l}$ . Then the symbol blocks are converted to a time domain by  $M_l$   $\bar{Q}$ -point inverse discrete Fourier transforms (IDFTs). After that, the cyclic prefix is added and then followed by an analog RF beamformer  $\mathbf{F}_A(t) \in \mathbb{C}^{N_l \times M_l}$ , which is common for all subcarriers. Finally, the signal transmitted at the  $q$ -th subcarrier can be written as:

$$\mathbf{x}_q(t) = \mathbf{F}_A(t) \mathbf{f}_{D,q}(t) s_q(t) \triangleq \mathbf{f}_q(t) s_q(t), \quad (4)$$

where  $\mathbf{f}_q(t) \triangleq \mathbf{F}_A(t) \mathbf{f}_{D,q}(t)$  denotes the hybrid precoding vector.

At each AP, the received signal is first combined with an RF combiner  $\mathbf{W}_A(t) \in \mathbb{C}^{N_r \times M_r}$ , which is common for all subcarriers. After the cyclic prefix is removed, the symbols are transformed to the frequency domain by  $M_r$   $\bar{Q}$ -point DFTs and then the symbols associated with the  $q$ -th subcarrier are combined by a digital baseband combining matrix  $\mathbf{W}_{D,q}(t) \in \mathbb{C}^{M_r \times M}$ , where  $M \leq M_r$ . With the assumption of perfect time synchronization, the received signal at the  $q$ -th subcarrier can finally be written as:

$$\mathbf{y}_q(t) = \mathbf{W}_{D,q}^H(t) \mathbf{W}_A^H(t) (\mathbf{H}_q(t) \mathbf{x}_q(t) + \mathbf{n}_q(t)) \triangleq \mathbf{W}_q^H(t) \mathbf{H}_q(t) \mathbf{f}_q(t) s_q(t) + \mathbf{W}_q^H(t) \mathbf{n}_q(t), \quad (5)$$

where  $\mathbf{W}_q(t) \triangleq \mathbf{W}_A(t) \mathbf{W}_{D,q}(t)$  denotes the hybrid combining matrix, and  $\mathbf{n}_q(t) \in \mathbb{C}^M, \sim \mathcal{CN}(0, \sigma_n^2)$  is the additive white Gaussian noise.

Our objective is to estimate the channel parameters including the complex gain, AoA, AoD, time delay and the Doppler shift for each path. After the channel parameters are estimated, the obtained channel state information is further used for estimating the location, speed and heading of the target vehicle. In the following section, we propose a novel training protocol that allows to express the received signal as a fourth-order tensor that admits a CPD.

## 3 Proposed Approach

### 3.1 CP Formulation

To facilitate the algorithmic development, we first propose a new frame structure, where each frame is divided into  $K_f$  subframes, and each subframe consists of  $P$  OFDM symbols. The first  $K$  subframes are used for channel estimation, and the rest  $K_f - K$  subframes are used for data transmission. For each frame, the frequency-domain channel associated with the  $q$ -th subcarrier at a certain time, e.g., at the  $p$ -th symbol of the  $(k+1)$ -th subframe, can be expressed as:

$$\mathbf{H}_q[(kP+p)T_{\text{sym}}] = \sum_{l=1}^L \beta_l \mathbf{a}_R(\phi_l) \mathbf{a}_T^H(\theta_l) e^{-j2\pi f_c \tau_l} e^{j2\pi \nu_l (kP+p)T_{\text{sym}}}. \quad (6)$$

For notational convenience,  $\mathbf{H}_q[(kP+p)T_{\text{sym}}]$  is also denoted by  $\mathbf{H}_q[k,p]$ . Similarly, we use  $\mathbf{F}_A[k,p]$ ,  $\mathbf{f}_{D,q}[k,p]$ , and  $s_q[k,p]$  to respectively represent  $\mathbf{F}_A[(kP+p)T_{\text{sym}}]$ ,  $\mathbf{f}_{D,q}[(kP+p)T_{\text{sym}}]$ , and  $s_q[(kP+p)T_{\text{sym}}]$ .

In the channel estimation stage, we suppose  $\mathbf{F}_A[k,p] = \mathbf{F}_A[p]$ ,  $\mathbf{f}_{D,q}[k,p] = \mathbf{f}_D[p]$  and  $s_q[k,p] = s[p] = 1$ . Thus, we have:

$$\mathbf{x}_q[k,p] = \mathbf{f}[p]. \quad (7)$$

Similarly, we suppose  $\mathbf{W}_A[k,p] = \mathbf{W}_A[p]$ ,  $\mathbf{W}_{D,q}[k,p] = \mathbf{W}_D[p]$ , and let  $\mathbf{W} = \mathbf{W}[p] \triangleq \mathbf{W}_A[p] \mathbf{W}_D[p]$ . Consequently, the received signal at the  $q$ -th symbol of the  $k$ -th subframe can be expressed as:

$$\mathbf{y}_q[k,p] = \mathbf{W}^H \mathbf{H}_q[k,p] \mathbf{f}[p] + \mathbf{W}^H \mathbf{n}_q[k,p]. \quad (8)$$

We define

$$\mathbf{H}_{q,l}[k] \triangleq \beta_l \mathbf{a}_R(\phi_l) \mathbf{a}_T^H(\theta_l) e^{-j2\pi f_c \tau_l} e^{j2\pi \nu_l k P T_{\text{sym}}}. \quad (9)$$

We can express  $\mathbf{H}_q[k,p]$  as:

$$\mathbf{H}_q[k,p] = \sum_{l=1}^L \mathbf{H}_{q,l}[k] e^{j2\pi \nu_l p T_{\text{sym}}}. \quad (10)$$

For each subcarrier, we collect signals received at each subframe and define  $\mathbf{Y}_{k,q} \triangleq [\mathbf{y}_q[k,1] \cdots \mathbf{y}_q[k,P]] \in \mathbb{C}^{M \times P}$ . We can express  $\mathbf{Y}_{k,q}$  as:

$$\mathbf{Y}_{k,q} = \sum_{l=1}^L \mathbf{W}^H \mathbf{H}_{q,l}[k] \mathbf{F} \mathbf{X}_{\nu_l} + \mathbf{N}_{k,q}, \quad (11)$$

where  $\mathbf{F} \triangleq [f[1] \cdots f[P]] \in \mathbb{C}^{N_l \times P}$ ,  $\mathbf{X}_{\nu_l} \triangleq \text{diag}(\tilde{\mathbf{g}}(\nu_l))$ , and

$$\tilde{\mathbf{g}}(\nu_l) \triangleq [e^{j2\pi \nu_l T_{\text{sym}}} \cdots e^{j2\pi \nu_l P T_{\text{sym}}}]^T \in \mathbb{C}^P. \quad (12)$$

Substituting Eq. (9) into Eq. (11), we obtain:

$$\begin{aligned} \mathbf{Y}_{k,q} &= \sum_{l=1}^L \beta_l e^{-j2\pi f_c \tau_l} e^{j2\pi \nu_l k P T_{\text{sym}}} \mathbf{W}^H \mathbf{a}_R(\phi_l) \mathbf{a}_T^H(\theta_l) \mathbf{F} \mathbf{X}_{\nu_l} + \mathbf{N}_{k,q} = \\ &= \sum_{l=1}^L \beta_l e^{-j2\pi f_c \tau_l} \mathbf{g}_k(\nu_l) \mathbf{W}^H \mathbf{a}_R(\phi_l) \mathbf{a}_T^H(\theta_l) \mathbf{F} \mathbf{X}_{\nu_l} + \mathbf{N}_{k,q} = \\ &= \sum_{l=1}^L \beta_l e^{-j2\pi f_c \tau_l} \mathbf{g}_k(\nu_l) \tilde{\mathbf{a}}_R(\phi_l) \tilde{\mathbf{a}}_T(\theta_l, \nu_l) + \mathbf{N}_{k,q}, \end{aligned} \quad (13)$$

where  $\tilde{\mathbf{a}}_T(\theta_l, \nu_l) \triangleq \mathbf{X}_{\nu_l}^H \mathbf{F}^H \mathbf{a}_T(\theta_l) \in \mathbb{C}^P$ ,  $\mathbf{g}_k(\nu_l) \triangleq e^{j2\pi \nu_l k P T_{\text{sym}}}$  and  $\tilde{\mathbf{a}}_R(\phi_l) \triangleq \mathbf{W}^H \mathbf{a}_R(\phi_l) \in \mathbb{C}^M$ .

For each subcarrier, the received signal collected from all  $K$  subframes can naturally be organized as a third-order tensor  $\mathcal{Y}_q \in \mathbb{C}^{M \times P \times K}$ . Note that each slice of the tensor  $\mathcal{Y}_q$ ,  $\mathbf{Y}_{k,q}$ , is a weighted sum of a common set of rank-one outer products. Therefore, the tensor  $\mathcal{Y}_q$  admits a CP decomposition

that decomposes a tensor into a sum of rank-one component tensors, i.e.,

$$\mathcal{Y}_q = \sum_{l=1}^L \beta_l e^{-j2\pi f_l \tau_l} \tilde{\mathbf{a}}_R(\phi_l) \circ \tilde{\mathbf{a}}_T(\theta_l, \nu_l) \circ \mathbf{g}(\nu_l) + \mathcal{N}_q, \quad (14)$$

where  $\mathbf{g}(\nu_l) \triangleq [e^{j2\pi\nu_l PT_{\text{sym}}} \dots e^{j2\pi\nu_l KPT_{\text{sym}}}]^T \in \mathbb{C}^K$ . Furthermore, the received signal associated with all  $Q$  subcarriers can be constructed as a fourth-order tensor  $\mathcal{Y} \in \mathbb{C}^{M \times P \times K \times Q}$ , which also admits a CP decomposition as follows.

$$\mathcal{Y} = \sum_{l=1}^L \tilde{\mathbf{a}}_R(\phi_l) \circ \tilde{\mathbf{a}}_T(\theta_l, \nu_l) \circ \mathbf{g}(\nu_l) \circ \beta_l \mathbf{f}(\tau_l) + \mathcal{N}, \quad (15)$$

where  $\mathbf{f}(\tau_l) \triangleq [e^{-j2\pi f_l \tau_l} \dots e^{-j2\pi f_l Q \tau_l}]^T \in \mathbb{C}^Q$ . The four modes of the tensor  $\mathcal{Y} \in \mathbb{C}^{M \times P \times K \times Q}$  stand for the received data stream, the OFDM symbol, the subframe and the subcarrier, respectively.

Due to the sparse scattering characteristics of mmWave channels, the CP rank of the fourth-order tensor, equivalent to the number of signal paths, is small. Therefore, it is expected that the CPD of  $\mathcal{Y}$  is unique for moderate values of  $M$ ,  $P$ ,  $K$ , and  $Q$ . Since the training overhead is equal to  $PKQ$ , it means that only a small amount of training overhead is needed to uniquely obtain the factor matrices of the tensor  $\mathcal{Y}$ . After the factor matrices are obtained, the channel parameters can be readily extracted. Before proceeding, we define the four factor matrices as:

$$\begin{aligned} \mathbf{A} &\triangleq [\tilde{\mathbf{a}}_R(\phi_1), \dots, \tilde{\mathbf{a}}_R(\phi_L)] \in \mathbb{C}^{M \times L}, \\ \mathbf{B} &\triangleq [\tilde{\mathbf{a}}_T(\theta_1, \nu_1), \dots, \tilde{\mathbf{a}}_T(\theta_L, \nu_L)] \in \mathbb{C}^{P \times L}, \\ \mathbf{C} &\triangleq [\mathbf{g}(\nu_1), \dots, \mathbf{g}(\nu_L)] \in \mathbb{C}^{K \times L}, \\ \mathbf{D} &\triangleq [\beta_1 \mathbf{f}(\tau_1), \dots, \beta_L \mathbf{f}(\tau_L)] \in \mathbb{C}^{Q \times L}. \end{aligned} \quad (16)$$

### 3.2 CP Decomposition

We commence with the number of paths which is known or has been estimated a priori. The CP decomposition of  $\mathcal{Y}$  can be accomplished by solving the following optimization problem.

$$\min_{\hat{\mathbf{A}}, \hat{\mathbf{B}}, \hat{\mathbf{C}}, \hat{\mathbf{D}}} \left\| \mathcal{Y} - \sum_{l=1}^L \hat{\mathbf{a}}_l \circ \hat{\mathbf{b}}_l \circ \hat{\mathbf{c}}_l \circ \hat{\mathbf{d}}_l \right\|_F^2, \quad (17)$$

where  $\hat{\mathbf{A}} = [\hat{\mathbf{a}}_1, \dots, \hat{\mathbf{a}}_L]$ ,  $\hat{\mathbf{B}} = [\hat{\mathbf{b}}_1, \dots, \hat{\mathbf{b}}_L]$ ,  $\hat{\mathbf{C}} = [\hat{\mathbf{c}}_1, \dots, \hat{\mathbf{c}}_L]$ ,  $\hat{\mathbf{D}} = [\hat{\mathbf{d}}_1, \dots, \hat{\mathbf{d}}_L]$  and  $\| \cdot \|_F$  denotes the Frobenius norm. The above optimization problem can be readily solved by an alternating least squares (ALS) procedure. Specifically, ALS alternatively minimizes the data fitting error with respect to one of the factor matrices, with the other three factor matrices fixed. The  $t$ -th iteration can proceed as

$$\begin{aligned} \hat{\mathbf{A}}^{(t+1)} &= \arg \min_{\hat{\mathbf{A}}} \left\| \mathcal{Y}_{(1)} - \hat{\mathbf{A}} \left( \hat{\mathbf{D}}^{(t-1)} \circ \hat{\mathbf{C}}^{(t-1)} \circ \hat{\mathbf{B}}^{(t-1)} \right)^T \right\|_F^2, \\ \hat{\mathbf{B}}^{(t+1)} &= \arg \min_{\hat{\mathbf{B}}} \left\| \mathcal{Y}_{(2)} - \hat{\mathbf{B}} \left( \hat{\mathbf{D}}^{(t)} \circ \hat{\mathbf{C}}^{(t)} \circ \hat{\mathbf{A}}^{(t)} \right)^T \right\|_F^2, \\ \hat{\mathbf{C}}^{(t+1)} &= \arg \min_{\hat{\mathbf{C}}} \left\| \mathcal{Y}_{(3)} - \hat{\mathbf{C}} \left( \hat{\mathbf{D}}^{(t)} \circ \hat{\mathbf{B}}^{(t)} \circ \hat{\mathbf{A}}^{(t)} \right)^T \right\|_F^2, \\ \hat{\mathbf{D}}^{(t+1)} &= \arg \min_{\hat{\mathbf{D}}} \left\| \mathcal{Y}_{(4)} - \hat{\mathbf{D}} \left( \hat{\mathbf{C}}^{(t)} \circ \hat{\mathbf{B}}^{(t)} \circ \hat{\mathbf{A}}^{(t)} \right)^T \right\|_F^2, \end{aligned} \quad (18)$$

where  $\mathcal{Y}_{(n)}$  denotes the mode- $n$  unfolding of  $\mathcal{Y}$ . Note the above least squares problems admit closed-form solutions, which are given by  $\hat{\mathbf{A}}^{(t+1)} = \mathcal{Y}_{(1)} \left( \left( \hat{\mathbf{D}}^{(t-1)} \circ \hat{\mathbf{C}}^{(t-1)} \circ \hat{\mathbf{B}}^{(t-1)} \right)^T \right)^\dagger$ ,  $\hat{\mathbf{B}}^{(t+1)} = \mathcal{Y}_{(2)} \left( \left( \hat{\mathbf{D}}^{(t)} \circ \hat{\mathbf{C}}^{(t)} \circ \hat{\mathbf{A}}^{(t)} \right)^T \right)^\dagger$ ,  $\hat{\mathbf{C}}^{(t+1)} = \mathcal{Y}_{(3)} \left( \left( \hat{\mathbf{D}}^{(t)} \circ \hat{\mathbf{B}}^{(t)} \circ \hat{\mathbf{A}}^{(t)} \right)^T \right)^\dagger$ , and  $\hat{\mathbf{D}}^{(t+1)} = \mathcal{Y}_{(4)} \left( \left( \hat{\mathbf{C}}^{(t)} \circ \hat{\mathbf{B}}^{(t)} \circ \hat{\mathbf{A}}^{(t)} \right)^T \right)^\dagger$ , respectively. The ALS iteration can proceed until the objective value of Eq. (17) is below a predefined threshold. If the knowledge of the number of paths,  $L$ , is unavailable, we adopt a multi-dimensional minimum description length (MDL) criterion to estimate the rank of the tensor<sup>[24-25]</sup>.

Without loss of generality, for an  $N$ -way tensor  $\mathcal{Y}$  with rank- $R$  corrupted by zero-mean circularly symmetric complex Gaussian (ZMCSCG) noise, we suppose that its CP decomposition is:

$$\mathcal{Y} = \sum_{r=1}^R \mathbf{a}_r^{(1)} \circ \mathbf{a}_r^{(2)} \circ \dots \circ \mathbf{a}_r^{(N)}. \quad (19)$$

Let  $M_n$  be the number of rows of the  $n$ -th factor matrix of  $\mathcal{Y}$  and the associated factor matrices are defined as  $\{\mathbf{A}^{(n)}\}_{n=1}^N$  with  $\mathbf{A}^{(n)} \in \mathbb{C}^{M_n \times R}$ . Let  $\tilde{M} \triangleq \prod_{n=1}^N M_n$ . Then for the  $n$ -mode unfolding of  $\mathcal{Y}$ , we compute the sample covariance matrix as:

$$\hat{\mathbf{R}}_{yy}^{(n)} = \frac{M_n}{\tilde{M}} [\mathcal{Y}_{(n)}][\mathcal{Y}_{(n)}]^H \in \mathbb{C}^{M_n \times M_n}. \quad (20)$$

Define  $\lambda_j^{(n)}$  as the  $j$ -th eigenvalue of the  $n$ -th sample covariance matrix  $\hat{\mathbf{R}}_{yy}^{(n)}$ , and we assume the  $M_n$  eigenvalues of  $\hat{\mathbf{R}}_{yy}^{(n)}$  are arranged in a descending order:

$$\lambda_1^{(n)} > \lambda_2^{(n)} > \dots > \lambda_{M_n}^{(n)}. \quad (21)$$

The estimation of the matrix rank of  $\mathcal{Y}_{(n)}$  can be given by the MDL criterion as

$\hat{R}^{(n)} = \arg \min_{\ell \in \{0, \dots, M_n - 1\}} \text{MDL}^{(n)}(\ell)$ , where

$$\text{MDL}^{(n)}(\ell) = \frac{\ell}{2} (2M_n - \ell) \log(\bar{M}^{(n)}) - \bar{M}^{(n)} (M_n - \ell) \log \left( \frac{\left( \prod_{j=\ell+1}^{M_n} \lambda_j^{(n)} \right)^{\frac{1}{M_n - \ell}}}{\frac{1}{M_n - \ell} \sum_{j=\ell+1}^{M_n} \lambda_j^{(n)}}} \right), \quad (22)$$

in which  $\bar{M}^{(n)} = \prod_{i=1, i \neq n}^N M_i$ . Finally, the rank of the tensor can be estimated as  $\hat{R} = \min \{ \hat{R}^{(n)} \}_{n=1}^N$ .

### 3.3 Estimation of Channel Parameters

We discuss how to estimate the parameters of the time-varying mmWave channel based on the estimated factor matrices  $\{\hat{\mathbf{A}}, \hat{\mathbf{B}}, \hat{\mathbf{C}}, \hat{\mathbf{D}}\}$ . Note that the CP decomposition is unique up to scaling and permutation ambiguity under a mild condition, as is detailed in the next subsection. More precisely, the relationship between the estimated and true factor matrices is established as follows:

$$\begin{aligned} \hat{\mathbf{A}} &= \mathbf{A} \mathbf{A}_1 \mathbf{I} + \mathbf{E}_1, \\ \hat{\mathbf{B}} &= \mathbf{B} \mathbf{A}_2 \mathbf{I} + \mathbf{E}_2, \\ \hat{\mathbf{C}} &= \mathbf{C} \mathbf{A}_3 \mathbf{I} + \mathbf{E}_3, \\ \hat{\mathbf{D}} &= \mathbf{D} \mathbf{A}_4 \mathbf{I} + \mathbf{E}_4, \end{aligned} \quad (23)$$

where  $\{\mathbf{A}_1, \mathbf{A}_2, \mathbf{A}_3, \mathbf{A}_4\}$  are unknown nonsingular diagonal matrices that satisfy  $\mathbf{A}_1 \mathbf{A}_2 \mathbf{A}_3 \mathbf{A}_4 = \mathbf{I}$ ,  $\mathbf{I}$  is an unknown permutation matrix, and  $\mathbf{E}_1, \mathbf{E}_2, \mathbf{E}_3$ , and  $\mathbf{E}_4$  denote the estimation errors associated with the four estimated factor matrices, respectively.

The permutation matrix  $\mathbf{I}$  can be ignored as it is common to all factor matrices. Note that the  $l$ -th column of  $\mathbf{A}$  and  $\mathbf{C}$  is determined by  $\hat{\phi}_l$  and  $\hat{\nu}_l$ , respectively. Hence the AoA and the Doppler shift can be estimated via a correlation-based method:

$$\hat{\phi}_l = \arg \max_{\phi_l} \frac{|\hat{\mathbf{a}}_l^H \tilde{\mathbf{a}}_R(\phi_l)|}{\|\hat{\mathbf{a}}_l\|_2 \|\tilde{\mathbf{a}}_R(\phi_l)\|_2}, \quad (24)$$

$$\hat{\nu}_l = \arg \max_{\nu_l} \frac{|\hat{\mathbf{c}}_l^H \mathbf{g}(\nu_l)|}{\|\hat{\mathbf{c}}_l\|_2 \|\mathbf{g}(\nu_l)\|_2}. \quad (25)$$

The  $l$ -th column of  $\mathbf{B}$  is characterized by both  $\hat{\theta}_l$  and  $\hat{\nu}_l$ . After the Doppler shift is estimated, we define  $\tilde{\mathbf{C}} \in \mathbb{C}^{P \times L}$  with  $[\tilde{\mathbf{C}}]_{p,l} = e^{j2\pi p T \nu_l}$ , and  $\tilde{\mathbf{B}} \in \mathbb{C}^{P \times L}$  with  $[\tilde{\mathbf{B}}]_{p,l} = [\hat{\mathbf{B}}]_{p,l} / [\tilde{\mathbf{C}}]_{p,l}$ .

Defining  $\check{\mathbf{a}}_T(\theta_l) \triangleq \mathbf{F}^H \mathbf{a}_T(\theta_l) \in \mathbb{C}^P$ , we can estimate the AoD as:

$$\hat{\theta}_l = \arg \max_{\theta_l} \frac{|\check{\mathbf{b}}_l^H \check{\mathbf{a}}_T(\theta_l)|}{\|\check{\mathbf{b}}_l\|_2 \|\check{\mathbf{a}}_T(\theta_l)\|_2}, \quad (26)$$

in which  $\check{\mathbf{b}}_l$  is the  $l$ -th column of  $\tilde{\mathbf{B}}$ . Also, we note that the  $l$ -th column of  $\mathbf{D}$  is  $\beta_l \mathbf{f}(\tau_l)$ . Hence the time delay  $\tau_l$  can be estimated via

$$\hat{\tau}_l = \arg \max_{\tau_l} \frac{|\hat{\mathbf{d}}_l^H \mathbf{f}(\tau_l)|}{\|\hat{\mathbf{d}}_l\|_2 \|\mathbf{f}(\tau_l)\|_2}, \quad (27)$$

where  $\hat{\mathbf{d}}_l$  denotes the  $l$ -th column of  $\hat{\mathbf{D}}$ .

Finally, we try to recover the complex path gain, given the estimated AoA, AoD, time delay and Doppler shift. We define the reconstructed factor matrices as follows.

$$\begin{aligned} \tilde{\mathbf{A}} &\triangleq [\tilde{\mathbf{a}}_R(\hat{\phi}_1), \dots, \tilde{\mathbf{a}}_R(\hat{\phi}_L)] \in \mathbb{C}^{M \times L}, \\ \tilde{\mathbf{B}} &\triangleq [\tilde{\mathbf{a}}_T(\hat{\theta}_1, \hat{\nu}_1), \dots, \tilde{\mathbf{a}}_T(\hat{\theta}_L, \hat{\nu}_L)] \in \mathbb{C}^{P \times L}, \\ \tilde{\mathbf{C}} &\triangleq [\mathbf{g}(\hat{\nu}_1), \dots, \mathbf{g}(\hat{\nu}_L)] \in \mathbb{C}^{K \times L}, \\ \tilde{\mathbf{D}} &\triangleq [\mathbf{f}(\hat{\tau}_1), \dots, \mathbf{f}(\hat{\tau}_L)] \in \mathbb{C}^{Q \times L}. \end{aligned} \quad (28)$$

Note that the reconstructed factor matrices share the same permutation ambiguity  $\mathbf{I}$ , and  $\tilde{\mathbf{D}}$  does not include the complex path gains. With the reconstructed  $\tilde{\mathbf{A}}, \tilde{\mathbf{B}}, \tilde{\mathbf{C}}$ , we can obtain an estimate of the true factor matrix  $\mathbf{D}$  by resorting to the mode-4 unfolding of  $\mathcal{Y}_{(4)}$ , i.e.

$$\check{\mathbf{D}} = \arg \min_{\check{\mathbf{D}}} \left\| \mathcal{Y}_{(4)} - \check{\mathbf{D}} (\tilde{\mathbf{C}} \circ \tilde{\mathbf{B}} \circ \tilde{\mathbf{A}})^T \right\|_F^2. \quad (29)$$

Define  $\check{\mathbf{Z}}_\beta = \text{diag}(\beta_1, \dots, \beta_L)$ . Theoretically we have

$$\hat{\check{\mathbf{Z}}}_\beta = \arg \min_{\check{\mathbf{Z}}_\beta} \left\| \check{\mathbf{D}} - \tilde{\mathbf{D}} \hat{\check{\mathbf{Z}}}_\beta \right\|_F^2. \quad (30)$$

Thus the complex path gains can be estimated via a least squares (LS) method

$$\hat{\beta}_l = [\tilde{\mathbf{D}}^\dagger \check{\mathbf{D}}]_{l,l}. \quad (31)$$

### 3.4 Uniqueness Condition and Sample Complexity

Clearly, the uniqueness of the CP decomposition is essential to the success of recovering channel parameters. In this subsection, we analyze the conditions that ensure the uniqueness of the CPD for our problem. The uniqueness conditions also shed light on the sample complexity (i.e. training overhead) required by the proposed algorithm.

A well-known condition for the uniqueness of CPD is

Kruskal's condition. Specifically, let  $k_X$  denote the  $k$ -rank of a matrix  $X$ , which is defined as the largest value of  $k_X$  so that every subset of  $k_X$  columns of the matrix  $X$  is linearly independent. We then have the following theorem concerning the uniqueness of CP decomposition for the  $N$ -th-order tensor, which is reported in Ref. [26].

Theorem 1: Let  $\chi$  be an  $N$ -way tensor with rank- $R$  and suppose that its CP decomposition is:

$$\chi = \sum_{r=1}^R \mathbf{a}_r^{(1)} \circ \mathbf{a}_r^{(2)} \circ \dots \circ \mathbf{a}_r^{(N)}. \quad (32)$$

Then a sufficient condition for the uniqueness is

$$\sum_{n=1}^N k_{A^{(n)}} \geq 2R + (N - 1). \quad (33)$$

Note that Kruskal's condition cannot hold, when  $R = 1$ . However, in that case, the uniqueness has been proved by Harshman. Kruskal's sufficient condition is also necessary for  $R = 2$  and  $R = 3$ , but not for  $R > 3$ .

From the above theorem, we know that if

$$k_A + k_B + k_C + k_D \geq 2L + 3, \quad (34)$$

then the CP decomposition of  $\mathcal{Y}$  is unique. We first examine the  $k$ -rank of  $\mathbf{D} = [\mathbf{f}(\tau_1), \dots, \mathbf{f}(\tau_L)] \mathbf{Z}_\beta$ , where  $\mathbf{f}(\tau_l)$  has a Vandermonde structure. Obviously,  $\mathbf{D}$  is a columnwise-scaled Vandermonde matrix, and its  $k$ -rank is thus given by  $k_D = \min\{Q, L\}$ .

Next, we examine the  $k$ -rank of  $\mathbf{A}$ . Note that

$$\mathbf{A} = \mathbf{W}^H [\mathbf{a}_R(\phi_1), \dots, \mathbf{a}_R(\phi_L)] \triangleq \mathbf{W}^H \mathbf{A}_R, \quad (35)$$

where  $\mathbf{A}_R \in \mathbb{C}^{N \times L}$  is a Vandermonde matrix under the ULA consideration. It was proved in Ref. [11] that for a randomly generated  $\mathbf{W}$ , the  $k$ -rank of  $\mathbf{A}$  is  $k_A = \min\{M, L\}$ .

We now study the  $k$ -rank of  $\mathbf{B}$ . The factor matrix  $\mathbf{B}$  is expressed as:

$$\mathbf{B} = \mathbf{G} * (\mathbf{F}^H [\mathbf{a}_T(\theta_1), \dots, \mathbf{a}_T(\theta_L)]) \triangleq \mathbf{G} * (\mathbf{F}^H \mathbf{A}_T), \quad (36)$$

where  $\mathbf{G} \in \mathbb{C}^{P \times L}$  with  $[\mathbf{G}]_{p,l} = e^{j2\pi p T_{\text{syn}} \nu_l}$ , and  $*$  denotes the Hadamard product. Note  $\mathbf{G}$  has a Vandermonde structure and its  $l$ -th column is characterized by the Doppler shift of the  $l$ -th path. For a randomly generated  $\mathbf{F} \in \mathbb{C}^{N_l \times P}$  with each of its elements uniformly chosen from a unit circle, we define  $b_{p,l} \triangleq [\mathbf{G}]_{p,l} \mathbf{f}_p^H \mathbf{a}_T(\theta_l)$  as the  $(p, l)$ -th entry of  $\mathbf{B}$ , where  $\mathbf{f}_p$  denotes the  $p$ -th column of  $\mathbf{F}$ . It can be verified that  $\mathbb{E}[b_{p,l}] = 0, \forall p, l$  and

$$\mathbb{E}[b_{p_1, l_1}^H b_{p_2, l_2}] = \begin{cases} 0, & p_1 \neq p_2, \\ \frac{e^{j2\pi T_{\text{syn}} p_1 (\nu_{l_2} - \nu_{l_1})}}{N_l^2} \mathbf{a}_T^H(\theta_{l_1}) \mathbf{a}_T(\theta_{l_2}), & p_1 = p_2. \end{cases} \quad (37)$$

According to the asymptotic orthogonality for ULA<sup>[27]</sup>,  $\mathbf{a}_T^H(\theta_{l_1}) \mathbf{a}_T(\theta_{l_2})/N_l$  converges to zero as  $N_l \rightarrow \infty$  with  $\theta_{l_1} \neq \theta_{l_2}$ . Thus, we can see that the elements of  $\mathbf{B}$  are uncorrelated with each other since different paths have distinct AoDs. As a result, the  $k$ -rank of  $\mathbf{B}$  is given as  $k_B = \min\{P, L\}$ .

As for  $k_C$ , it can be easily verified that  $k_C = 1$  when the vehicle is stationary. Moreover,  $\mathbf{C}$  is a Vandermonde matrix for non-stationary vehicles, in which case we have  $k_C = \min\{K, L\}$ .

Finally, based on the above analysis, the Kruskal's condition is equivalent to

$$\min\{M, L\} + \min\{Q, L\} + \min\{P, L\} + \min\{K, L\} \geq 2L + 3. \quad (38)$$

For a small  $L$ , we can reasonably assume that the number of subcarriers is greater than  $L$ , say,  $Q \geq L$ . Also, if we assume  $M$ , the dimension of the combining matrix  $\mathbf{W}_{D,q}(t)$ , is greater than 2, that is  $M \geq 2$ , we only need to ensure  $\min\{P, L\} + \min\{K, L\} \geq L + 1$ . Such a condition can be easily satisfied by setting either  $K = 1, P \geq L$  or  $P = 1, K \geq L$ .

Note that the training overhead required by the proposed method is  $PKQ$ . From the above discussion, it is easy to know that the amount of training overhead is in the order of  $\mathcal{O}(L^2)$ . Due to the sparse scattering characteristics of mmWave channels,  $L$  is usually small. Hence the proposed method can achieve reliable channel estimates with a moderate amount of training overhead.

## 4 Vehicle Sensing Based on Channel Estimates

In V2I systems, based on the estimated channel parameters, multiple APs can collaborate to localize a target vehicle and estimate its related kinematic parameters such as the heading and speed of the vehicle. These estimated positions and kinematic parameters can be used to assist the communication between the vehicle and APs, such as beam switching and beam tracking. On the other hand, these APs can construct a real-time traffic map based on the positions and kinematic parameters of different vehicles, which can be used to give driving suggestions to vehicles, such as traffic jams ahead, vehicle formation, follow-up, and lane change, so that the traffic efficiency is enhanced<sup>[28]</sup>.

For simplicity, we consider a two-dimensional Cartesian coordinate system (CCS) as illustrated in Fig. 1, where the orientation of each AP's antenna array is assumed to be parallel with the  $y$ -axis. The locations of the  $n$ -th AP and the ve-

hicle are respectively denoted as

$$\begin{aligned} \mathbf{p}_{\text{AP}}^n &= [x_{\text{AP}}^n, y_{\text{AP}}^n]^T \in \mathbb{R}^2, \\ \mathbf{p}_v &= [x_v, y_v]^T \in \mathbb{R}^2, \end{aligned} \quad (39)$$

where  $\mathbf{p}_{\text{AP}}^n$  is known while  $\mathbf{p}_v$  is to be estimated. In addition, there is an unknown vehicle heading, namely the orientation of the vehicle's antenna array, which is denoted by  $\alpha \in [0, \frac{\pi}{2})$ , and the speed of the vehicle in this direction is denoted as  $v$ .

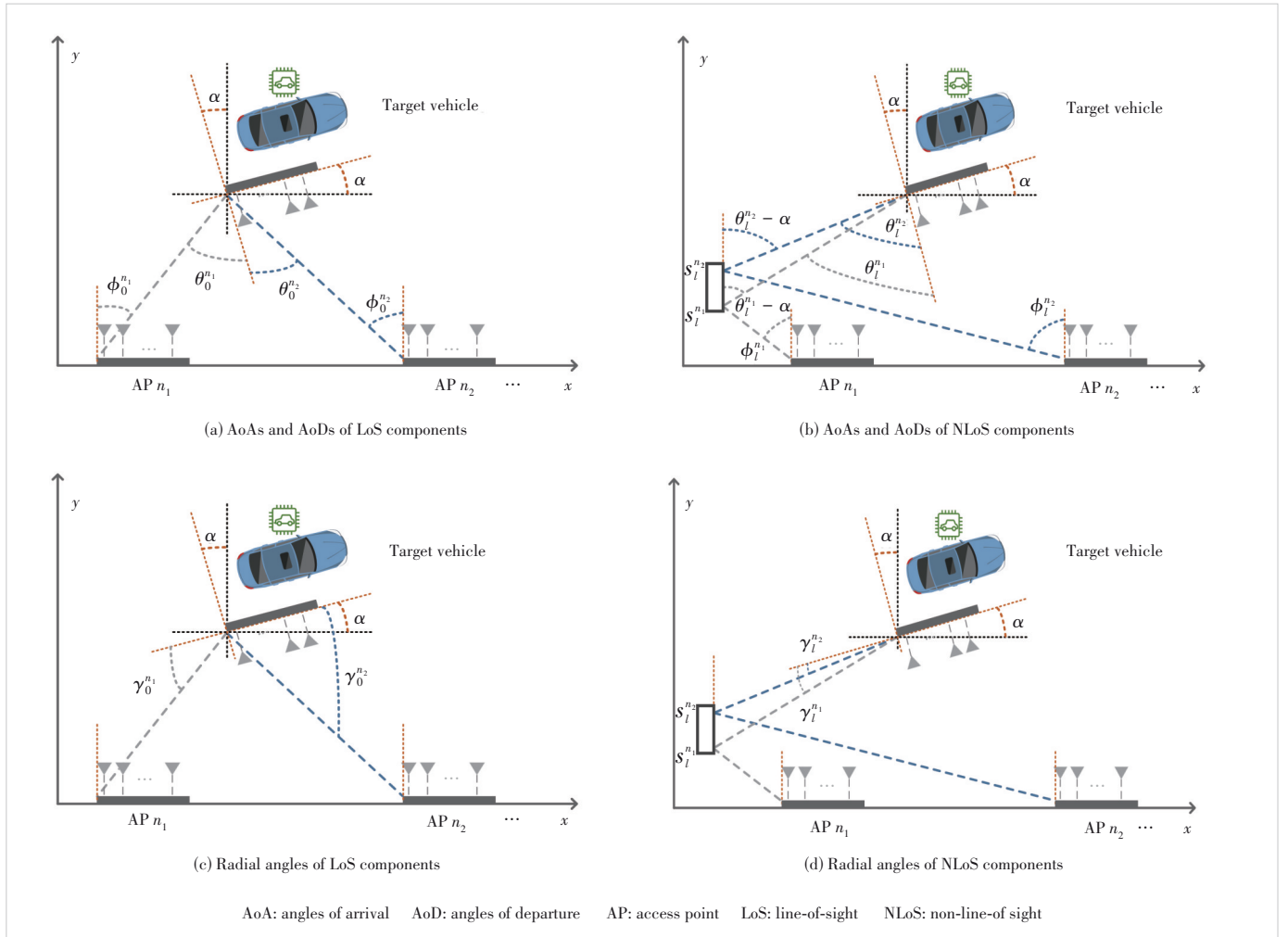
For each AP, like the  $n$ -th AP, we assume there exists a LOS path and  $L_n - 1$  non-line-of sight (NLOS) paths. The  $l$ -th ( $l > 0$ ) NLOS path is a result of a scatterer at an unknown location:

$$\mathbf{p}_s^{n,l} = [x_s^{n,l}, y_s^{n,l}]^T \in \mathbb{R}^2. \quad (40)$$

Note that for different APs, different paths may corre-

spond to the same scatterer. For the uplink scenario, from the geometric relationship delineated in Figs. 1(a) and 1(b), the time delay, AoD, and AoA of each path and the positions of the vehicle/AP can be expressed as

$$\begin{aligned} \tau_0^n &= \frac{\|\mathbf{p}_{\text{AP}}^n - \mathbf{p}_v\|_2}{c}, \\ \tau_l^n &= \frac{\|\mathbf{p}_{\text{AP}}^n - \mathbf{p}_s^{n,l}\|_2 + \|\mathbf{p}_v - \mathbf{p}_s^{n,l}\|_2}{c}, \quad l > 0, \\ \phi_0^n &= \arctan\left(\frac{x_v - x_{\text{AP}}^n}{y_v - y_{\text{AP}}^n}\right), \\ \phi_l^n &= \arctan\left(\frac{x_s^{n,l} - x_{\text{AP}}^n}{y_s^{n,l} - y_{\text{AP}}^n}\right), \quad l > 0, \\ \theta_0^n &= \phi_0^n + \alpha, \\ \theta_l^n &= \arctan\left(\frac{x_v - x_s^{n,l}}{y_v - y_s^{n,l}}\right) + \alpha, \quad l > 0, \end{aligned} \quad (41)$$



▲ Figure 1. A schematic for Vehicle-to-Infrastructure (V2I) coordinate systems

where  $\phi_l^n \in \left(-\frac{\pi}{2}, \frac{\pi}{2}\right)$ , and  $\theta_l^n \in \left(-\frac{\pi}{2}, \frac{\pi}{2}\right)$ .

To portray the motion relationship between the target vehicle and APs, we define the radial angle  $\gamma_l^n \in [0, \frac{\pi}{2}]$ ,  $l \geq 0$ , as shown in Figs. 1(c) and 1(d). For the LoS path, the radial angle can be calculated as:

$$\gamma_0^n = \begin{cases} \frac{\pi}{2} + \phi_0^n + \alpha, & x_v \leq x_{\text{AP}}^n (\phi_0^n \leq 0); \\ \frac{\pi}{2} - \phi_0^n - \alpha, & x_v > x_{\text{AP}}^n (\phi_0^n > 0). \end{cases} \quad (42)$$

For the NLoS path, the radial angle can be calculated as

$$\gamma_l^n = \begin{cases} \frac{\pi}{2} + \phi_l^n + \alpha, & x_v \leq x_s^{n,l} (\phi_l^n \leq 0); \\ \frac{\pi}{2} - \phi_l^n - \alpha, & x_v > x_s^{n,l} (\phi_l^n > 0). \end{cases} \quad (43)$$

Note that  $\gamma_l^n$  ( $l > 0$ ) is actually the radial angle between the target vehicle and the scatterer  $s_l^n$ , so that the radial velocity between the target vehicle and the scatterer  $s_l^n$  can be regarded as the radial velocity between the target vehicle and the  $n$ -th AP under the assumption that all scatterers are static or quasi-static.

According to the kinematic relation between the vehicle and the  $n$ -th AP, the radial velocity of the target vehicle concerning the  $n$ -th AP can be expressed as:

$$v_l^n = \begin{cases} v \cos \gamma_l^n, & \text{toward AP movement;} \\ -v \cos \gamma_l^n, & \text{reverse AP movement,} \end{cases} \quad (44)$$

where  $l \geq 0$ . Obviously, based on achieving super-resolution channel estimation, highly accurate target vehicle localization and motion state (including heading and velocity) can be perceived via channel parameters.

#### 4.1 Case of Single AP

For the proposed V2I mmWave MIMO OFDM system, after the channel estimation stage, we can reap the channel parameters from the target vehicle to all APs so that the location and motion of the target vehicle can be perceived through the geometric relationship. We define  $\{\hat{\theta}_l^n, \hat{\phi}_l^n, \hat{\beta}_l^n, \hat{\tau}_l^n, \hat{\nu}_l^n\}_{l=0}^{L_n-1}$  as the estimated channel path parameters from the vehicle to the  $n$ -th AP, where  $l = 0$  means the LoS components of the  $n$ -th link. The vehicle's position and heading can be consequently given as

$$\begin{aligned} \hat{\mathbf{p}}_v^n &= \mathbf{p}_{\text{AP}}^n + \hat{\tau}_0^n c [\sin \hat{\phi}_0^n, \cos \hat{\phi}_0^n]^T, \\ \hat{\alpha}^n &= \hat{\theta}_0^n - \hat{\phi}_0^n, \end{aligned} \quad (45)$$

and then the first-order reflection  $s_l^n$  can be reasonably acquired by the intersection of the straight lines that respec-

tively start from the AP's and vehicle's location, i.e.

$$\begin{aligned} \hat{x}_s^{n,l} &= x_{\text{AP}}^n + (y_s^{n,l} - y_{\text{AP}}^n) \tan \hat{\phi}_l^n, \quad l > 0, \\ \hat{y}_s^{n,l} &= \frac{x_{\text{AP}}^n - \hat{x}_v + y_v \tan(\hat{\theta}_l^n - \hat{\alpha}) - y_{\text{AP}}^n \tan \hat{\phi}_l^n}{\tan(\hat{\theta}_l^n - \hat{\alpha}) - \tan \hat{\phi}_l^n}, \quad l > 0. \end{aligned} \quad (46)$$

Next, the radial degree between the vehicle and the  $n$ -th anchor can be calculated as:

$$\hat{\gamma}_0^n = \begin{cases} \frac{\pi}{2} + \hat{\phi}_0^n + \hat{\alpha}, & \hat{x}_v \leq x_{\text{AP}}^n; \\ \frac{\pi}{2} - \hat{\phi}_0^n - \hat{\alpha}, & \hat{x}_v > x_{\text{AP}}^n. \end{cases} \quad (47)$$

and the estimated vehicle velocity at the  $n$ -th AP is:

$$\hat{v}^n = \frac{\hat{\nu}_0^n}{\cos \hat{\gamma}_0^n}, \quad (48)$$

where  $\hat{\nu}_0^n = \hat{\nu}_0^n c / f_c$ , and  $\hat{\nu}_0^n$  is the estimated Doppler shift from the LoS component. Moreover, it can be inferred the target vehicle moves toward the  $n$ -th AP if  $\hat{v}^n > 0$  and vice versa.

#### 4.2 Case of Multi-APs

For the case of multi-APs, we have the estimated time-varying channel parameters as  $\{\hat{\theta}_l^n, \hat{\phi}_l^n, \hat{\beta}_l^n, \hat{\tau}_l^n, \hat{\nu}_l^n\}_{l=0, n=1}^{L_n-1, N}$ . For a LoS path, the location of targets is determined only by the path delay and AoA with respect to the related AP, hence we develop the estimation of the vehicle's location from the estimated path delays and AoAs of all LoS paths between the vehicle and APs. For simplicity, we ignore the subscript of the LoS path, and define the mapping as follows.

$$\boldsymbol{\eta}^n(\mathbf{p}_v) \triangleq \left[ \arctan \left( \frac{x_v - x_{\text{AP}}^n}{y_v - y_{\text{AP}}^n} \right), \frac{\|\mathbf{p}_{\text{AP}}^n - \mathbf{p}_v\|_2}{c} \right]^T. \quad (49)$$

For the  $n$ -th AP,  $n = 1, \dots, N$ , we have

$$\hat{\boldsymbol{\eta}}^n = \boldsymbol{\eta}^n(\mathbf{p}_v) + \boldsymbol{\omega}^n, \quad (50)$$

where  $\hat{\boldsymbol{\eta}}^n = [\hat{\phi}^n, \hat{\tau}^n]^T$ , and  $\boldsymbol{\omega}^n$  is the measurement error. Without loss of generality, we assume  $\boldsymbol{\omega} \triangleq [[\boldsymbol{\omega}^1]^T, \dots, [\boldsymbol{\omega}^N]^T]^T$  is distributed with mean zero and covariance  $\boldsymbol{\Sigma}_\omega$ . Define  $\boldsymbol{\eta}(\mathbf{p}_v) \triangleq [[\boldsymbol{\eta}^1(\mathbf{p}_v)]^T, \dots, [\boldsymbol{\eta}^N(\mathbf{p}_v)]^T]^T \in \mathbb{R}^{2N}$ ,  $\hat{\boldsymbol{\eta}} \triangleq [[\hat{\boldsymbol{\eta}}^1]^T, \dots, [\hat{\boldsymbol{\eta}}^N]^T]^T \in \mathbb{R}^{2N}$ , and the estimation of the target location from multi-APs can be formulized as the following nonlinear weighted least-square (WLS) problem, i.e.

$$\begin{aligned} \hat{\mathbf{p}} &= \arg \min_{\mathbf{p}} [\hat{\boldsymbol{\eta}} - \boldsymbol{\eta}(\mathbf{p})]^T \mathbf{R} [\hat{\boldsymbol{\eta}} - \boldsymbol{\eta}(\mathbf{p})] \\ \text{s.t. } &\mathbf{p} \in \mathcal{D}_v, \end{aligned} \quad (51)$$

where  $\mathcal{D}_v$  denotes the location range of the target vehicle and  $\mathbf{R}$  can be chosen as  $\mathbf{R} = \mathbf{I}$  or  $\mathbf{R} = \Sigma_\omega$  [29].

Next, we develop the Gauss-Newton method to iteratively solve Problem (51), which approximates the mapping  $\boldsymbol{\eta}(\mathbf{p})$  by the first-order Taylor-series expansion at a given point  $\mathbf{p}^{(0)}$  as:

$$\begin{aligned} \boldsymbol{\eta}(\mathbf{p}) &\approx \boldsymbol{\eta}(\mathbf{p}^{(0)}) + \mathbf{J}(\mathbf{p}^{(0)})(\mathbf{p} - \mathbf{p}^{(0)}), \\ \mathbf{J}(\mathbf{p}^{(0)}) &= \left. \frac{\partial \boldsymbol{\eta}(\mathbf{p})}{\partial \mathbf{p}} \right|_{\mathbf{p}=\mathbf{p}^{(0)}}. \end{aligned} \quad (52)$$

The nonlinear WLS Problem (51) can be converted to

$$\begin{aligned} \hat{\mathbf{p}} &= \arg \min_{\mathbf{p}} \left[ \hat{\boldsymbol{\eta}} - \boldsymbol{\eta}(\mathbf{p}^{(0)}) - \mathbf{J}(\mathbf{p}^{(0)})(\mathbf{p} - \mathbf{p}^{(0)}) \right]^T \mathbf{R} \times \\ &\quad \left[ \hat{\boldsymbol{\eta}} - \boldsymbol{\eta}(\mathbf{p}^{(0)}) - \mathbf{J}(\mathbf{p}^{(0)})(\mathbf{p} - \mathbf{p}^{(0)}) \right] \\ \text{s.t. } &\mathbf{p} \in \mathcal{D}_v, \end{aligned} \quad (53)$$

and the estimate of  $\mathbf{p}_v$  at the  $(t+1)$ -th iteration can be obtained by

$$\hat{\mathbf{p}}^{(t+1)} = \hat{\mathbf{p}}^{(t)} + \left( \mathbf{J}^T(\mathbf{p}^{(t)}) \mathbf{R} \mathbf{J}(\mathbf{p}^{(t)}) \right)^{-1} \mathbf{J}^T(\mathbf{p}^{(t)}) \boldsymbol{\Delta}(\mathbf{p}^{(t)}), \quad (54)$$

where  $\boldsymbol{\Delta}(\mathbf{p}^{(t)}) = (\hat{\boldsymbol{\eta}} - \boldsymbol{\eta}(\mathbf{p}^{(t)}))$ . The above iteration can proceed until the convergence condition  $\|\boldsymbol{\Delta}(\mathbf{p}^{(t)})\| < \varepsilon$  is met, where  $\varepsilon$  is a predefined stopping threshold. Moreover, we can project the finally iterated result to  $\mathcal{D}_v$  and make a significant location estimation of the target vehicle.

Defining  $\hat{\mathbf{p}}_v = [\hat{x}_v, \hat{y}_v]^T$  as the estimate of the vehicle's location by Eq. (53), we then discuss how to obtain the vehicle's heading  $\alpha$  and velocity  $v$ . Specifically, we first reconstruct the observation of AoD at all APs as:

$$\tilde{\phi}^n = \arctan \left( \frac{\hat{x}_v - x_{\text{AP}}^n}{\hat{y}_v - y_{\text{AP}}^n} \right), \quad n = 1, \dots, N, \quad (55)$$

with which we have a series of remodeled heading as

$$\tilde{\alpha}^n = \hat{\theta}^n - \tilde{\phi}^n, \quad n = 1, \dots, N. \quad (56)$$

Let  $\tilde{\boldsymbol{\eta}}_\alpha \triangleq [\tilde{\alpha}^1, \dots, \tilde{\alpha}^N]^T$ , and an LS estimator of  $\alpha$  can be given as

$$\begin{aligned} \hat{\alpha} &= \arg \min_{\alpha} \left\| \tilde{\boldsymbol{\eta}}_\alpha - \boldsymbol{\eta}_\alpha \right\|_2^2 \\ \text{s.t. } &\boldsymbol{\eta}_\alpha = \mathbf{1} \cdot \alpha \\ &\alpha \in \mathcal{D}_\alpha, \end{aligned} \quad (57)$$

where  $\mathcal{D}_\alpha$  denotes the angle range of the vehicle's heading.

The LS solution can be easily obtained as  $\hat{\alpha} = \frac{1}{N} \sum_{n=1}^N \tilde{\alpha}^n$ .

Furthermore, we have a similar way to remodel the obser-

vation of radial angles at all APs as:

$$\tilde{\gamma}^n = \begin{cases} \frac{\pi}{2} + \tilde{\phi}^n + \hat{\alpha}, & \hat{x}_v \leq x_{\text{AP}}^n; \\ \frac{\pi}{2} - \tilde{\phi}^n - \hat{\alpha}, & \hat{x}_v > x_{\text{AP}}^n, \end{cases} \quad (58)$$

with which we have  $\tilde{v}^n = \frac{\hat{v}^n \cdot c}{\cos \tilde{\gamma}^n \cdot f_c}$ , where  $\hat{v}^n$  is the estimated Doppler shift from the LoS component of the channel between the  $n$ -th AP and the vehicle. Let  $\tilde{\boldsymbol{\eta}}_v \triangleq [|\tilde{v}^1|, \dots, |\tilde{v}^N|]^T$ , and an LS estimator of  $v$  can be given as

$$\begin{aligned} \hat{v} &= \arg \min_v \left\| \tilde{\boldsymbol{\eta}}_v - \boldsymbol{\eta}_v \right\|_2^2 \\ \text{s.t. } &\boldsymbol{\eta}_v = \mathbf{1} \cdot v \\ &v \in \mathcal{D}_v, \end{aligned} \quad (59)$$

where  $\mathcal{D}_v$  denotes the velocity range of the vehicle. The LS solution can be easily obtained as  $\hat{v} = \frac{1}{N} \sum_{n=1}^N |\tilde{v}^n|$ .

## 5 Simulation Results

In this section, we carry out experiments to illustrate the performance of our proposed method. In simulations, the AP is located at  $\mathbf{p}_{\text{AP}} = [21, 0]^T$ . The vehicle is located at  $\mathbf{p}_v = [43, 8]^T$  and moving with a heading  $\alpha = \frac{\pi}{12}$  and a radial velocity  $v = 40$  km/h toward the AP. The number of paths  $L = 3$  and we consider a distance-dependent path loss. For the LoS path ( $l = 0$ ),  $\beta_0 \sim CN(0, 10^{-0.1\kappa})$ , and  $\kappa = a + 10b \log_{10}(D) + \xi$ , in which  $D$  denotes the distance between the vehicle and the AP, and  $\xi \sim N(0, \sigma_\xi^2)$ . The values of  $a, b, \sigma_\xi$  are set to be  $a = 61.4$  dB,  $b = 2$  dB and  $\sigma_\xi = 5.8$  dB as suggested by LoS real-world channel measurement [30]. For the NLoS path ( $l > 0$ ), the complex path gain is  $\beta_l \sim CN(0, 10^{-0.1(\kappa + \mu)})$ , and  $\mu$  is the Rician factor [31–32]. The carrier frequency is 28 GHz unless otherwise stated. There are  $N_t = 32$  antennas at the vehicle (transmitter),  $N_r = 64$  antennas and  $M_r = 6$  RF chains at each AP. The total number of subcarriers is  $\bar{Q} = 100$ , out of which  $Q = 10$  subcarriers are selected for training, and the sampling rate is set to  $f_s = 100$  MHz. The number of subframes for training is set to  $K = 3$ , and the number of symbols in one subframe is set to  $P = 10$ . The beamforming matrices  $\mathbf{F}$  and  $\mathbf{W}$  are randomly generated with their entries uniformly chosen from a unit circle. The signal-to-noise ratio (SNR) is defined as:

$$\text{SNR} = \frac{\left\| \mathbf{y} - \mathcal{N} \right\|_F^2}{\left\| \mathcal{N} \right\|_F^2}, \quad (60)$$

where  $\mathcal{Y}$  and  $\mathcal{N}$  denote the received signal and the additive noise. The performance of our proposed method is evaluated by the mean square error (MSE), which is defined as

$$\text{MSE}(\mathbf{s}) = \sum_{l=1}^L |\mathbf{s}_l - \hat{\mathbf{s}}_l|^2, \quad (61)$$

where  $\mathbf{s}_l \in \{\theta_l, \phi_l, \tau_l, \nu_l, \beta_l\}$  and the MSE is calculated separately to examine the estimation accuracy for each parameter. We also leverage the Cramer-Rao bound (CRB) results for a baseline of the estimates of channel parameters. The CRB is a lower bound on the variance of any biased estimator<sup>[33]</sup>. It provides a benchmark for evaluating the performance of our proposed method.

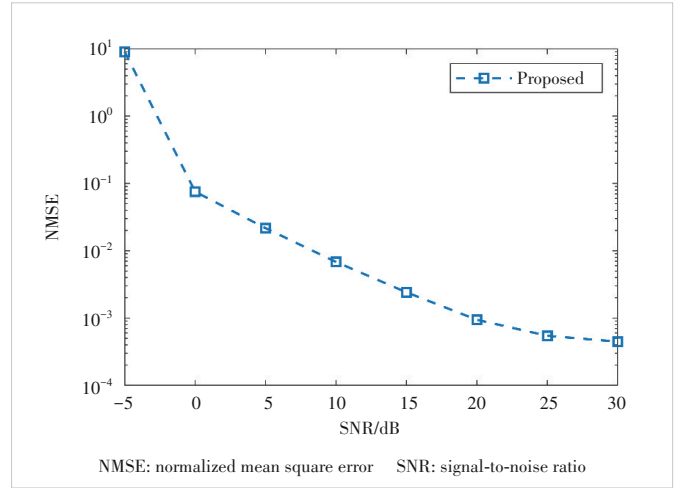
The performance of our proposed method as a function of SNR is depicted in Fig. 2. It can be observed that the CRBs of all five parameters decrease exponentially against the increased SNR. In addition, the MSEs of our proposed method converge to their lower bound while the SNR is increasing, which validates the efficacy of the proposed method for channel estimation. Specifically, the MSEs of AoA, AoD, Doppler shift and time delay are relatively close to its CRB, while the gap between the MSE and CRB of path gain is relatively wider, which may be subject to accumulated estimation errors.

In Fig. 3, we show the normalized mean square error

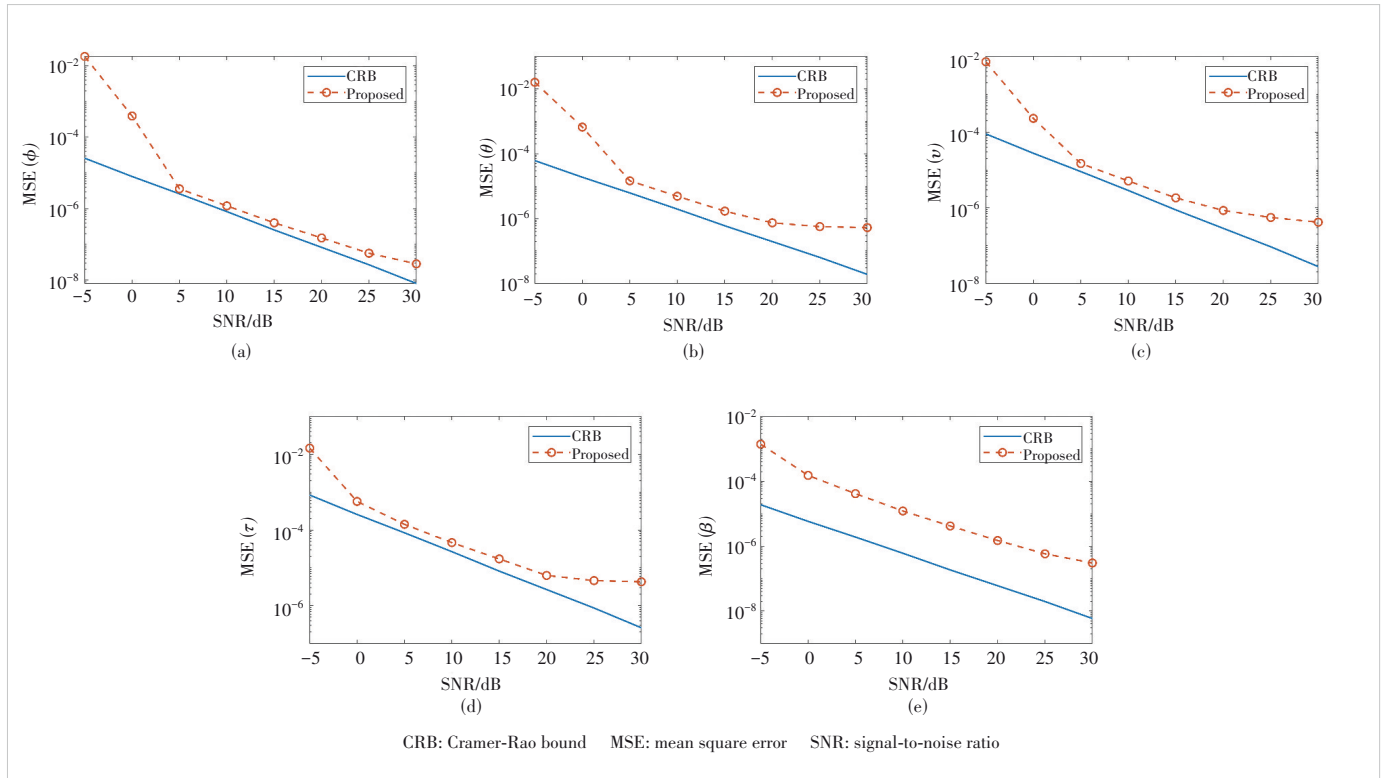
(NMSE) result for our proposed method as a function of SNR, in which the NMSE is defined by:

$$\text{NMSE} = \frac{\sum_{q=1}^Q \|\mathbf{H}_q - \hat{\mathbf{H}}_q\|_F^2}{\sum_{q=1}^Q \|\mathbf{H}_q\|_F^2}, \quad (62)$$

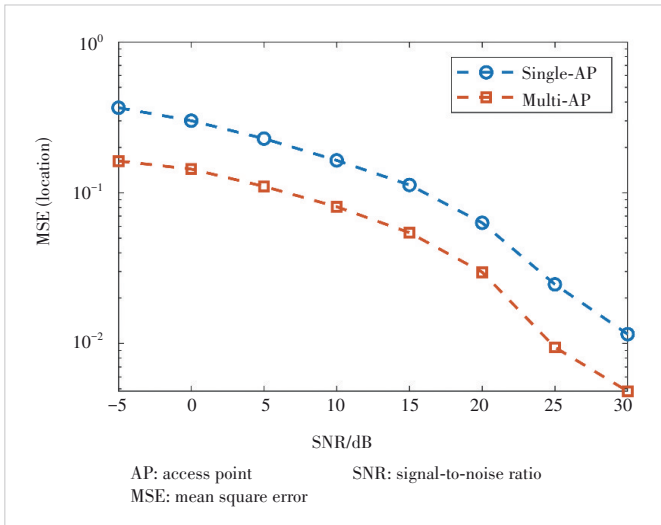
where  $\mathbf{H}_q$  denotes the frequency-domain channel matrix as-



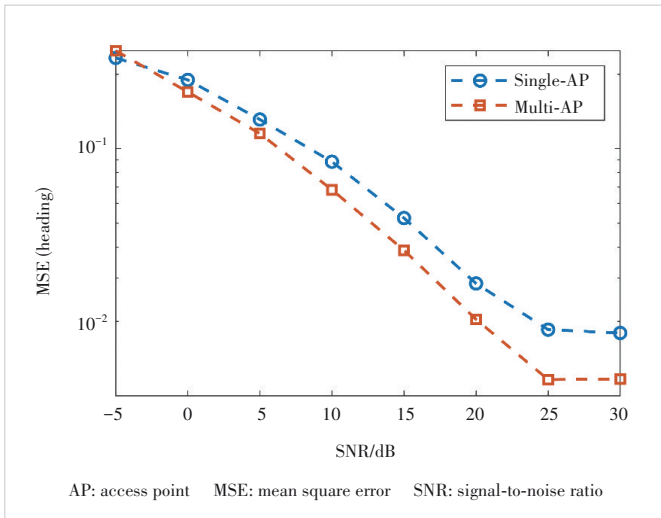
▲ Figure 3. Channel estimation performance versus SNR



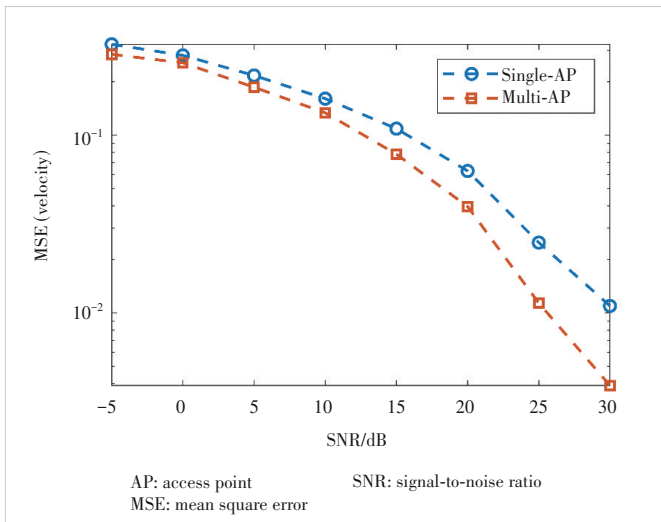
▲ Figure 2. MSEs and CRBs associated with different parameters versus SNR



▲ Figure 4. MSEs of vehicle's location versus SNR



▲ Figure 5. MSEs of vehicle's heading versus SNR



▲ Figure 6. MSEs of vehicle's velocity versus SNR

sociated with the  $q$ -th subcarrier, and  $\hat{H}_q$  is its estimate. Thanks to accurate channel parameter estimation, the proposed method can deliver a relatively accurate channel estimate as long as the SNR is above 0 dB.

Based on the estimation of channel parameters, the location, heading and velocity of the vehicle can be recovered from the geometric relationship as well as the motion relationship between the vehicle and each AP. To fully illustrate sensing performance, we compare the sensing performance of two cases namely single-AP and multi-AP for the V2I system. Specifically, we consider AP1 is located at  $p_{AP}^1 = [21, 0]^T$  and AP2 is located at  $p_{AP}^2 = [82, 0]^T$ . The vehicle is located at  $p_v = [58, 12]^T$  and moving with a heading  $\alpha = \frac{\pi}{12}$  and a radial velocity  $v = 50$  km/h toward AP2. The sensing performance of the two cases is plotted in Figs. 4, 5 and 6, from which we can observe that the sensing performance of the multi-AP case outperforms that of the single-AP case. The performance improvement can be intuitively explained. Because the vehicle is closer to AP2, the channel link between vehicle-AP2 is stronger than vehicle-AP1, which yields more accurate channel parameter estimation. In particular, the wider performance gap in estimating the vehicle's location between the multi-AP case and the single-AP case is caused by the accumulation of errors, as the location estimation is based on both AoA and time delay estimates.

## 6 Conclusions

In this paper, a CP decomposition-based method is proposed for high-accuracy channel estimation as well as sensing in mmWave MIMO-OFDM V2I Systems. To characterize the Doppler shift due to the vehicle's mobility, a time-varying frequency-domain mmWave channel is derived, a novel frame structure is introduced and a CP decomposition-based channel estimator is proposed. Utilizing the estimates of channel parameters in multi-APs, a nonlinear weighted least-square problem is proposed to accurately recover the location, heading and velocity of the vehicle. Simulation results are carried out to illustrate the effectiveness of the proposed method in performing communication and sensing in mmWave MIMO-OFDM V2I Systems.

## Acknowledgement:

We would like to thank Prof. FANG Jun who led our team and helped revise this paper.

## References

- [1] RAPPAPORT T S, MURDOCK J N, GUTIERREZ F. State of the art in 60-GHz integrated circuits and systems for wireless communications [J]. Proceedings of the IEEE, 2011, 99(8): 1390 - 1436. DOI: 10.1109/JPROC.2011.2143650

- [2] RANGAN S, RAPPAPORT T S, ERKIP E. Millimeter-wave cellular wireless networks: Potentials and challenges [J]. *Proceedings of the IEEE*, 2014, 102(3): 366 – 385. DOI: 10.1109/JPROC.2014.2299397
- [3] GHOSH A, THOMAS T A, CUDAK M C, et al. Millimeter-wave enhanced local area systems: a high-data-rate approach for future wireless networks [J]. *IEEE journal on selected areas in communications*, 2014, 32(6): 1152 – 1163. DOI: 10.1109/JSAC.2014.2328111
- [4] YANG G, XIAO M, GROSS J, et al. Delay and backlog analysis for 60 GHz wireless networks [C]//*Proceedings of IEEE Global Communications Conference (GLOBECOM)*. IEEE, 2016: 1 – 7. DOI: 10.1109/GLOCOM.2016.7841725
- [5] SWINDLEHURST A L, AYANOGLU E, HEYDARI P, et al. Millimeter-wave massive MIMO: the next wireless revolution? [J]. *IEEE communications magazine*, 2014, 52(9): 56 – 62. DOI: 10.1109/MCOM.2014.6894453
- [6] ALKHATEEB A, EL AYACH O, LEUS G, et al. Channel estimation and hybrid precoding for millimeter wave cellular systems [J]. *IEEE journal of selected topics in signal processing*, 2014, 8(5): 831 – 846. DOI: 10.1109/JSTSP.2014.2334278
- [7] ALKHATEEB A, LEUS G, HEATH R W. Compressed sensing based multi-user millimeter wave systems: how many measurements are needed? [C]//*IEEE International Conference on Acoustics, Speech and Signal Processing (ICASSP)*. IEEE, 2015: 2909 – 2913. DOI: 10.1109/ICASSP.2015.7178503
- [8] ZHAO L, NG D W K, YUAN J H. Multi-user precoding and channel estimation for hybrid millimeter wave systems [J]. *IEEE journal on selected areas in communications*, 2017, 35(7): 1576 – 1590. DOI: 10.1109/JSAC.2017.2699378
- [9] VENUGOPAL K, ALKHATEEB A, GONZÁLEZ PRELCIC N, et al. Channel estimation for hybrid architecture-based wideband millimeter wave systems [J]. *IEEE journal on selected areas in communications*, 2017, 35(9): 1996 – 2009. DOI: 10.1109/JSAC.2017.2720856
- [10] ZHOU Z, FANG J, YANG L X, et al. Channel estimation for millimeter-wave multiuser MIMO systems via PARAFAC decomposition [J]. *IEEE transactions on wireless communications*, 2016, 15(11): 7501 – 7516. DOI: 10.1109/TWC.2016.2604259
- [11] ZHOU Z, FANG J, YANG L X, et al. Low-rank tensor decomposition-aided channel estimation for millimeter wave MIMO-OFDM systems [J]. *IEEE journal on selected areas in communications*, 2017, 35(7): 1524 – 1538. DOI: 10.1109/JSAC.2017.2699338
- [12] SONG H, FANG X M, FANG Y G. Millimeter-wave network architectures for future high-speed railway communications: Challenges and solutions [J]. *IEEE wireless communications*, 2016, 23(6): 114 – 122. DOI: 10.1109/MWC.2016.1500255WC
- [13] XIAO Z Y, XIA P F, XIA X G. Enabling UAV cellular with millimeter-wave communication: potentials and approaches [J]. *IEEE communications magazine*, 2016, 54(5): 66 – 73. DOI: 10.1109/MCOM.2016.7470937
- [14] CHOI J, VA V, GONZALEZ-PRELCIC N, et al. Millimeter-wave vehicular communication to support massive automotive sensing [J]. *IEEE communications magazine*, 2016, 54(12): 160 – 167. DOI: 10.1109/MCOM.2016.1600071CM
- [15] QIN Q B, GUI L, CHENG P, et al. Time-varying channel estimation for millimeter wave multiuser MIMO systems [J]. *IEEE transactions on vehicular technology*, 2018, 67(10): 9435 – 9448. DOI: 10.1109/TVT.2018.2854735
- [16] CHENG L, YUE G R, YU D Z, et al. Millimeter wave time-varying channel estimation via exploiting block-sparse and low-rank structures [J]. *IEEE access*, 2019, 7: 123355 – 123366. DOI: 10.1109/ACCESS.2019.2937628
- [17] SANCHIS P, MARTINEZ J M, HERRERA J, et al. A novel simultaneous tracking and direction of arrival estimation algorithm for beam-switched base station antennas in millimeter-wave wireless broadband access networks [C]//*IEEE Antennas and Propagation Society International Symposium*. IEEE, 2002: 594 – 597. DOI: 10.1109/APS.2002.1016415
- [18] DENG H, SAYEED A. Mm-wave MIMO channel modeling and user localization using sparse beamspace signatures [C]//*The 15th International Workshop on Signal Processing Advances in Wireless Communications (SPAWC)*. IEEE, 2014: 130 – 134. DOI: 10.1109/SPAWC.2014.6941331
- [19] VARI M, CASSIOLI D. mmWaves RSSI indoor network localization [C]//*IEEE International Conference on Communications Workshops (ICC)*. IEEE, 2014: 127 – 132. DOI: 10.1109/ICCW.2014.6881184
- [20] HU A Z, LV T J, GAO H, et al. An ESPRIT-based approach for 2-D localization of incoherently distributed sources in massive MIMO systems [J]. *IEEE journal of selected topics in signal processing*, 2014, 8(5): 996 – 1011. DOI: 10.1109/JSTSP.2014.2313409
- [21] GUERRA A, GUIDI F, DARDARI D. Position and orientation error bound for wideband massive antenna arrays [C]//*IEEE International Conference on Communication Workshop (ICCW)*. IEEE, 2015: 853 – 858. DOI: 10.1109/ICCW.2015.7247282
- [22] ALKHATEEB A, HEATH R W. Frequency selective hybrid precoding for limited feedback millimeter wave systems [J]. *IEEE transactions on communications*, 2016, 64(5): 1801 – 1818. DOI: 10.1109/TCOMM.2016.2549517
- [23] BAJWA W U, HAUPT J, SAYEED A M, et al. Compressed channel sensing: A new approach to estimating sparse multipath channels [J]. *Proceedings of the IEEE*, 2010, 98(6): 1058 – 1076. DOI: 10.1109/JPROC.2010.2042415
- [24] DA COSTA J P C L, ROEMER F, HAARDT M, et al. Multi-dimensional model order selection [J]. *EURASIP journal on advances in signal processing*, 2011, 2011(1): 26. DOI: 10.1186/1687-6180-2011-26
- [25] LIN Y X, JIN S, MATTHAIU M, et al. Tensor-based channel estimation for millimeter wave MIMO-OFDM with dual-wideband effects [J]. *IEEE transactions on communications*, 2020, 68(7): 4218 – 4232. DOI: 10.1109/TCOMM.2020.2983673
- [26] KRUSKAL J B. Three-way arrays: Rank and uniqueness of trilinear decompositions, with application to arithmetic complexity and statistics [J]. *Linear algebra and its applications*, 1977, 18(2): 95 – 138. DOI: 10.1016/0024-3795(77)90069-6
- [27] CHEN J H. When does asymptotic orthogonality exist for very large arrays? [C]//*IEEE Global Communications Conference (GLOBECOM)*. IEEE, 2013: 4146 – 4150. DOI: 10.1109/GLOCOM.2013.6831723
- [28] YANG Y, HUA K. Emerging technologies for 5G-enabled vehicular networks [J]. *IEEE access*, 2019, 7: 181117 – 181141. DOI: 10.1109/ACCESS.2019.2954466
- [29] LI Q, LAN J, ZHANG L, et al. Augmented nonlinear least squares estimation with applications to localization [J]. *IEEE transactions on aerospace and electronic systems*, 2022, 58(2): 1042 – 1054. DOI: 10.1109/TAES.2021.3115566
- [30] AKDENIZ M R, LIU Y P, SAMIMI M K, et al. Millimeter wave channel modeling and cellular capacity evaluation [J]. *IEEE journal on selected areas in communications*, 2014, 32(6): 1164 – 1179. DOI: 10.1109/JSAC.2014.2328154
- [31] YING K K, GAO Z, LYU S X, et al. GMD-based hybrid beamforming for large reconfigurable intelligent surface assisted millimeter-wave massive MIMO [J]. *IEEE access*, 2020, 8: 19530 – 19539. DOI: 10.1109/ACCESS.2020.2968456
- [32] SAMIMI M K, MACCARTNEY G R, SUN S, et al. 28 GHz millimeter-wave ultrawideband small-scale fading models in wireless channels [C]//*Proceedings of IEEE 83rd Vehicular Technology Conference (VTC Spring)*. IEEE, 2016: 1 – 6. DOI: 10.1109/VTC-Spring.2016.7503970
- [33] KAY S M. *Fundamentals of statistical signal processing* [M]. Englewood Cliffs, NJ: Prentice-Hall PTR, 1993

### Biographies

**WANG Jilin** (jilinwang@std.uestc.edu.cn) has been working toward his PhD degree with National Key Laboratory of Wireless Communications, University of Electronic Science and Technology of China (UESTC) since 2021. His current research interests include compressed sensing and millimeter-wave communication.

**ZENG Xianlong** received his BS degree from University of Electronic Science and Technology of China (UESTC) in 2018. He has been working toward his MS degree with National Key Laboratory of Wireless Communications, UESTC since 2022. His current research interests include integrated sensing and communication (ISAC).

**YANG Yonghui** received his BS degree in information countermeasure techniques and MS degree in electronic information engineering from Xidian University, China in 2006 and 2010, respectively. Since 2010, he has been with ZTE Corporation, where his research interests focus on wireless communications. His current research interests include 5G and 6G technology, and

millimeter-wave and terahertz communication.

**PENG Lin** received his BS degree in information engineering and MS degree in electromagnetic field and microwave techniques from Nanjing University of Science and Technology, China in 2004 and 2006, respectively. Since 2006, he has been with ZTE Corporation, where he focuses on the research of wireless communications. His current research interests include beyond 5G and 6G technology, millimeter-wave and terahertz communications and intelligent reflecting surface for wireless applications.

**LI Lingxiang** received her BS degree from Central South University, China in 2010, and her PhD degree from University of Electronic Science and Technology of China (UESTC) in 2017, all in electrical engineering. She was a visiting PhD student under supervision of Prof. Athina P. PETROPULU at Rutgers, The State University of New Jersey, USA during 2015 – 2016. Dr. LI is now an associate professor with the National Key Lab of Science and Technology on Communications, UESTC. Her research interests include THz communications and Integrated Sensing and Communications (ISAC).